# Nucleosynthesis of Elements in Low to Intermediate Mass Stars through the AGB Phase

John C. Lattanzio and Arnold I. Boothroyd

*Dept. of Mathematics, Monash University, Clayton, VIC. 3168, Australia*

**Abstract.**
   We present a review of the main phases of stellar evolution with particular emphasis on the nucleosynthesis and mixing mechanisms in low- and intermediate-mass stars. In addition to explicit studies of the effects of the first, second and third dredge-up, we also discuss *cool bottom processing* and *hot bottom burning*.

## I   INTRODUCTION

   In recent years a wealth of new abundance data has been obtained, both from stellar abundance observations and from precise laboratory measurements of isotope ratios in stellar grains from meteorites. This places strong constraints on nucleosynthesis and mixing in low and intermediate mass stars. A quantitative understanding relies on our knowledge of both the stellar evolution and the nucleosynthesis occurring in the stars.

   There are specific phases of a star's life where mixing brings to the surface the products of interior nucleosynthesis. These are referred to as "dredge-up" events, and there are basically three, although the details are mass-dependent. There are also observations which require mixing beyond what is found in the standard theory. This paper aims to review these events, both qualitatively, for non-experts, and quantitatively, for those more familiar with the area.

## II   BASIC STELLAR EVOLUTION

   In this section we give a qualitative overview of the evolution of stars of masses 1 and 5 $M_\odot$, with emphasis on the mechanisms and phenomenology of the structural and evolutionary changes. We consider in detail the evolution up to the beginning of thermal pulses on the AGB (the "TP-AGB"), with a brief discussion of further evolution (which is discussed in detail in section IV).

# A    Basic Evolution at 1 Solar Mass

We make the usual assumption that a star reaches the zero-age main sequence with a homogeneous chemical composition. Figure 1 shows a schematic HR diagram for a $\sim 1\ M_\odot$ star. Core H-burning occurs radiatively, and the central temperature and density grow in response to the increasing molecular weight (points 1–3) until central H exhaustion (point 4). The H profiles are shown in inset (a) in Figure 1. The star now leaves the main sequence and crosses the Hertzsprung Gap (points 5–7), while the central $^4$He-core becomes electron degenerate and the nuclear burning is established in a surrounding shell. Inset (b) shows the advance of the H-shell during this evolution. Simultaneously, the star is expanding and the outer layers become convective. As the star reaches the Hayashi limit ($\sim$ point 7), convection extends quite deeply inward (in mass) from the surface, and the star ascends the (first) red giant branch (RGB). The convective envelope penetrates into the region where partial H-burning has occurred earlier in the evolution, as shown in inset (c) of Figure 1. This material is still mostly H, but with added $^4$He together with the products of CN cycling, primarily $^{14}$N and $^{13}$C. These are now mixed to the surface (point 8); this phase is known as the *"first dredge-up"*. The most important surface abundance changes are an increase in the $^4$He mass fraction by $\sim 0.03$ (for masses $\lesssim 4\ M_\odot$), while $^{14}$N increases at the expense of $^{12}$C by $\sim 30\%$, and the number ratio $^{12}$C/$^{13}$C drops from its initial value of $\sim 90$ to lie between 18 and 26 [18]. Further details are given in section III below.

As the star ascends the giant branch the $^4$He-core continues to contract and heat. Neutrino energy losses from the centre cause the temperature maximum to move outward, as shown in inset (d) of Figure 1. Eventually triple-alpha reactions are ignited at this point of maximum temperature, but with a degenerate equation of state. The temperature and density are decoupled, and the resulting ignition is violent — the "core helium flash" (point 9: see, e.g., [21]). Following this, the star quickly moves to the Horizontal Branch where it burns $^4$He gently in a convective core, and H in a shell (which provides most of the luminosity). This corresponds to points 10–13 in Figure 1. Helium burning increases the mass fraction of $^{12}$C and $^{16}$O (the latter through $^{12}$C$(\alpha,\gamma)^{16}$O) and the outer regions of the convective core become stable to the Schwarzschild convection criterion but unstable to that of Ledoux: a situation referred to as "semiconvection" (space prohibits a discussion of this phenomenon, but an excellent physical description is contained in [14,15]). The semiconvection causes the composition profile to adjust itself to produce convective neutrality, with the resulting profiles as shown in inset (e) of Figure 1.

Following $^4$He exhaustion (point 14), the star ascends the giant branch for the second time, and this is known as the Asymptotic Giant Branch, or AGB, phase. The final proportions of $^{12}$C and $^{16}$O in the $^4$He-exhausted core depend on the uncertain rate for the $^{12}$C$(\alpha,\gamma)^{16}$O reaction. The core now becomes electron degenerate, and the star's energy output is provided by the $^4$He-
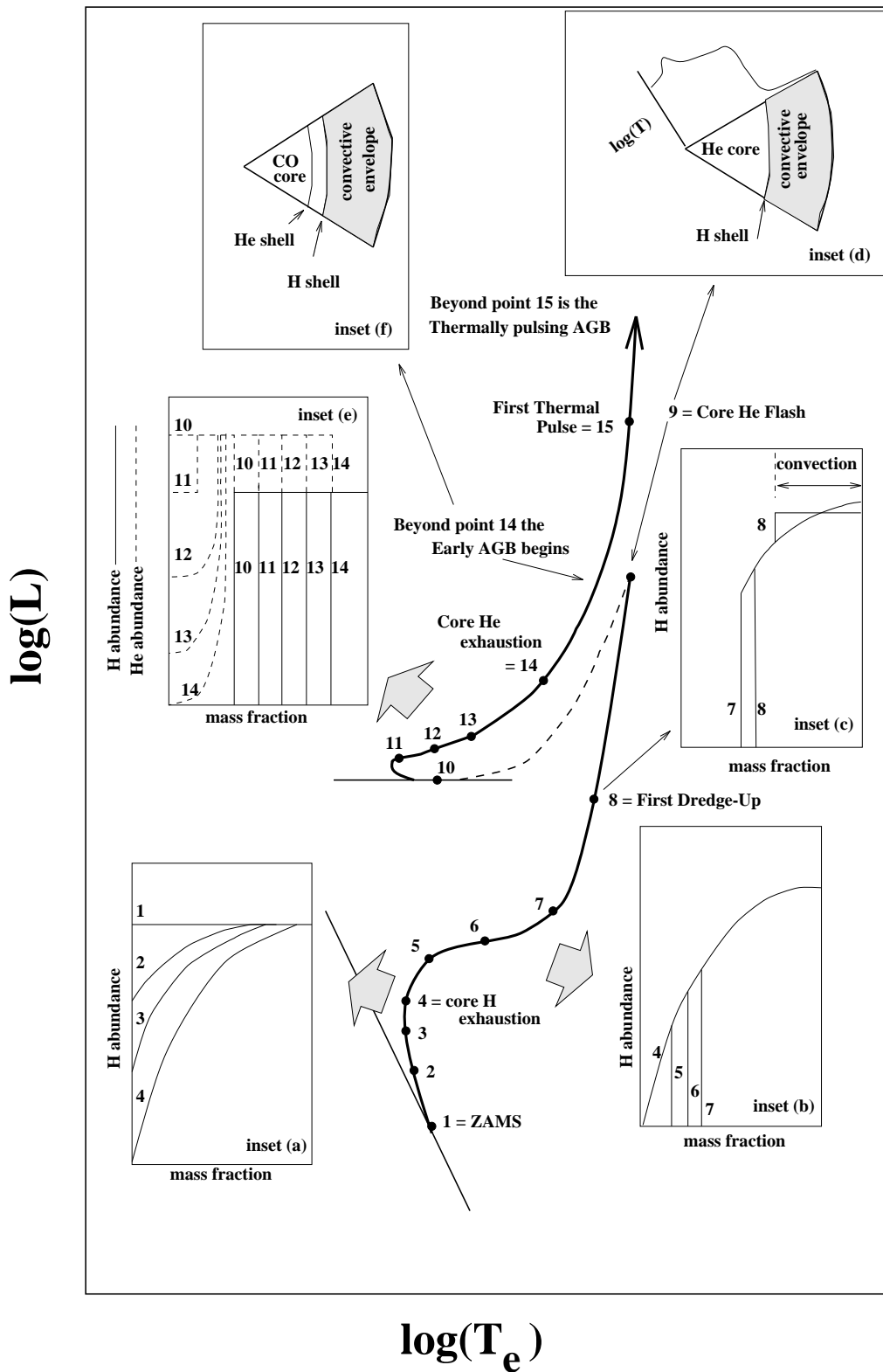
**FIGURE 1.** Schematic of evolution at $\sim 1 M_\odot$.

burning shell (which lies immediately above the C-O core) and the H-burning shell. Above both is the deep convective envelope. This structure is shown in inset (f) in Figure 1. We will later see that the $^4$He-shell is thermally unstable, as witnessed by the recurring "thermal pulses". Thus the AGB is divided into two regions: the early-AGB (E-AGB), prior to (and at lower luminosities than) the first thermal pulse, and the thermally-pulsing AGB (TP-AGB) beyond this. We will return to this in section IV.
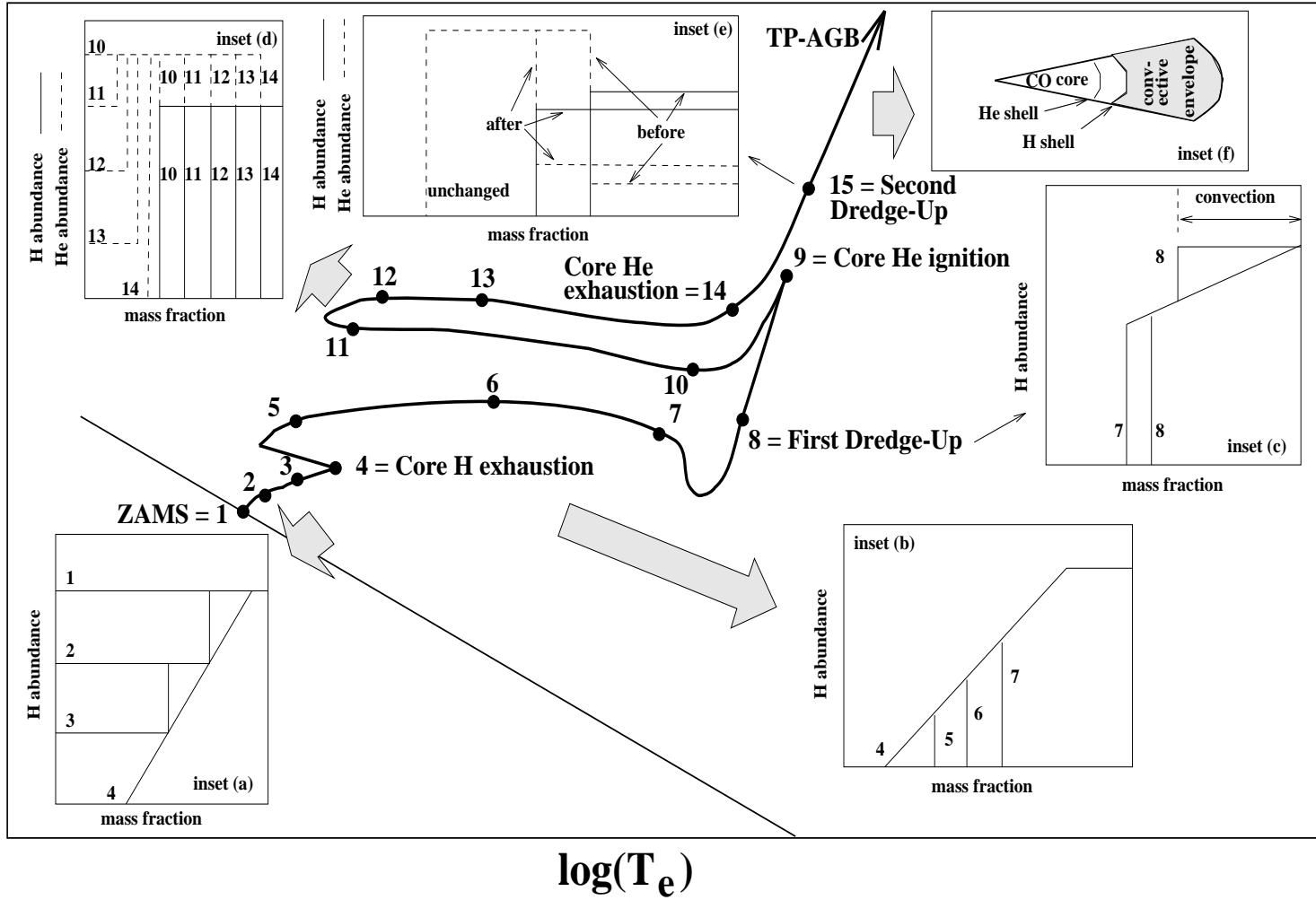
## B    Basic Evolution at 5 Solar Masses

A more massive star, say of $5M_\odot$, begins its life very similarly to the lower mass star discussed above. The main initial difference is that the higher temperature in the core causes CNO cycling to be the main source of H-burning, and the high temperature dependence of these reactions causes a convective core to develop. As H is burned into $^4$He the opacity (mainly owing to electron scattering, and hence proportional to the H content) decreases and the extent of the convective core decreases with time. This corresponds to points 1–4 in Figure 2. Following core H exhaustion there is a phase of shell burning as the star crosses the Hertzsprung Gap (points 5–7 and inset (b)), and then ascends the (first) giant branch. Again the inward penetration of the convective envelope (point 8) reaches regions where there has been partial H-burning earlier in the evolution, and thus these products (primarily $^{13}$C and $^{14}$N, produced at the cost of $^{12}$C) are mixed to the surface in the first dredge-up, just as seen at lower masses, and sketched in inset (c) of Figure 2.

For these more massive stars the ignition of $^4$He occurs in the centre and under non-degenerate conditions, and the star settles down to a period of quiescent $^4$He-burning in a convective core, together with H-burning in a shell (see inset (d) in Figure 2). The competition between these two energy sources determines the occurrence and extent of the subsequent blueward excursion in the HR diagram [58], when the star crosses the instability strip and is observed as a Cepheid variable (points 10–14). Following core $^4$He exhaustion, the structural re-adjustment to shell $^4$He burning results in a strong expansion, and the H-shell is extinguished as the star begins its ascent of the AGB. With this entropy barrier removed, the inner edge of the convective envelope is free to penetrate the inactive H-shell; the products of complete H-burning are mixed to the surface in "*second dredge-up*" (point 15). This again alters the surface compositions of $^4$He, $^{12}$C, $^{13}$C, and $^{14}$N, and reduces the mass of the H-exhausted core, (the process of mixing $^4$He outward also mixes H inward: see inset (e) in Fig. 2). There is a critical mass (of $\sim 4\ M_\odot$, but dependent on composition) below which the second dredge-up does not occur. Following second dredge-up, the H-shell is re-ignited, and the first thermal pulse occurs soon after: the star has reached the thermally-pulsing AGB, or TP-AGB. Note that at this stage the structure is qualitatively similar for all masses.

**FIGURE 2.** Schematic of evolution at $\sim 5 M_\odot$.

The figure shows a Hertzsprung-Russell diagram with axes $\log(T_e)$ (horizontal) and $\log(L)$ (vertical), tracing stellar evolution through labeled points:

- ZAMS = 1
- 2, 3
- 4 = Core H exhaustion
- 5, 6, 7
- 8 = First Dredge-Up
- 9 = Core He ignition
- 10, 11, 12, 13
- Core He exhaustion = 14
- 15 = Second Dredge-Up
- TP-AGB

Insets:
- inset (a): H abundance vs mass fraction, points 1, 2, 3, 4
- inset (b): H abundance vs mass fraction, points 4, 5, 6, 7
- inset (c): H abundance vs mass fraction, points 7, 8, with convection
- inset (d): H abundance / He abundance vs mass fraction, points 10, 11, 12, 13, 14
- inset (e): H abundance / He abundance vs mass fraction, before/after/unchanged
- inset (f): CO core, He shell, H shell, convective envelope

# C   The Key Mixing Events

As we saw above, when a star approaches the RGB after the completion of main sequence core H-burning, its convective envelope deepens, eventually dredging up products of partial H-burning (*first dredge-up*). The first dredge-up ceases when the convective envelope reaches its maximum inward penetration, and then recedes again. This leaves behind a sharp composition discontinuity. For low mass stars ($\lesssim 2.5\,M_\odot$), the H-burning shell catches up to and erases this discontinuity while the star is still on the RGB; for higher masses, the star leaves the RGB before this can take place. There is observational evidence from surface abundance changes on the RGB [31,32,38,54,75,49,48,18] (see section III) that, once the composition discontinuity is erased, some form of non-convective "*extra mixing*" takes place, which transports material from the (relatively cool) bottom of the convective envelope down close to the H-burning shell (where nuclear burning can alter its composition) and then up to be mixed back into the convective envelope. Boothroyd *et al.* [12] referred to this process as "*cool bottom processing*"; the mixing mechanism is not well understood, but is frequently assumed to be rotation-induced, e.g., meridional circulation [81] and/or shear-induced turbulence [19] (similar to the extra mixing process on the main sequence that yields large $^7$Li-depletions in $\sim 1\,M_\odot$ stars [63]). Note that "extra mixing" or "extra deep mixing" generally result in "cool bottom processing" and hence in surface abundance changes; these three terms are used essentially synonymously hereafter.

Low mass stars experience significant mass loss on the RGB (totaling $\sim 0.2\,M_\odot$), with peak mass loss rates of $\dot{M} \sim 10^{-7}\,M_\odot/\text{yr}$ near the tip of the RGB; some grain formation may take place during this stage.

After the completion of core He-burning, helium burns in a shell surrounding the degenerate carbon–oxygen core; the star ascends the AGB, and the convective envelope deepens again. In intermediate mass stars, the H-burning shell is temporarily extinguished and envelope convection reaches into and below the position of the H-shell, bringing more nucleosynthesized material to the surface (*second dredge-up*). This occurs on the early AGB (E-AGB). Afterwards, the H-shell re-ignites, and periodic thermal pulses (or helium shell flashes) occur — the thermally-pulsing AGB, or TP-AGB (see section IV). The strong nuclear energy generation in these thermal pulses causes a convective region to grow outwards from the He-burning shell, mixing the products of partial He-burning (mostly $^{12}$C) and of neutron-capture nucleosynthesis ("*s*-process isotopes") outwards almost to the base of the H-burning shell. Subsequently, the convective envelope reaches into the intershell region where the products of He-burning were deposited and mixes them to the surface (*third dredge-up*: see section V). Note that the third dredge-up is a repeating phenomenon, occurring after almost every pulse (except for the first few). This is in contrast to the first and second dredge-up events, which occur at most once per star (low mass stars do not experience the second dredge-up at all).

In stars with masses $\gtrsim 4\,M_\odot$, the convective envelope is deep enough during the long interpulse periods that it reaches into the H-burning shell, i.e., nuclear processing takes place at the bottom of the convective envelope, altering its composition. This is known as "*hot bottom burning*" (see section VI).

The AGB stage of evolution ends when mass loss has removed almost all of the star's envelope (the "planetary nebula" stage follows). In the "superwind" which terminates the AGB, mass loss rates of $\dot{M} \sim 10^{-4}\,M_\odot/\mathrm{yr}$ are observed; such dense outflows from cool stars are favorable sites for grain formation.

# III   THE RGB AND E-AGB: FIRST AND SECOND DREDGE-UP, AND EXTRA MIXING

Theoretical models of first and second dredge-up without any "extra mixing" or "cool bottom processing" [20,74,13,18,23,9] agree with each other reasonably well (see, e.g., Fig. 4); results presented here are from the models of Boothroyd & Sackmann [7,70,71,9]. For solar metallicity ($Z = 0.02$), solar elemental and isotopic abundances were assumed to represent the initial stellar composition. The $\alpha$-element enhancement at lower metallicity was approximated by setting $[\mathrm{O/Fe}] = -0.5\,[\mathrm{Fe/H}]$ for $[\mathrm{Fe/H}] > -1$, and constant $[\mathrm{O/Fe}] = +0.5$ for $[\mathrm{Fe/H}] \leq -1$; $[\mathrm{C/Fe}]$ and $[\mathrm{N/Fe}]$ were taken to be independent of metallicity, as indicated by observations (see Timmes *et al.* [84], and references therein). The initial isotopic ratios $^{12}\mathrm{C}/^{13}\mathrm{C}$, $^{16}\mathrm{O}/^{17}\mathrm{O}$, and $^{16}\mathrm{O}/^{18}\mathrm{O}$ were taken to be inversely proportional to Fe/H, as suggested by the galactic chemical evolution models of Timmes *et al.* [84,83] (there are few observational constraints on the evolution of these isotopic ratios in the interstellar medium). Nuclear rates from Caughlan & Fowler [17] were used, except for $^{12}\mathrm{C}(\alpha,\gamma)$ (where the rate was multiplied by 1.7, as recommended by Weaver & Woosley [89]), and $^{17}\mathrm{O}(\mathrm{p},\alpha)$ and $^{17}\mathrm{O}(\mathrm{p},\gamma)$, where the 1990 rates of Landré *et al.* [51] or the (slightly higher) 1995 rates of Blackmon *et al.* [4,3] were used. A value of the mixing length to pressure scale height ratio of $\alpha = 2.1$ was required in order to obtain a correct model of the Sun [70,71] (note that the value of $\alpha$ has almost no effect on the depth of dredge-up, as has already been noted by Charbonnel [18]). Reimers-formula red giant mass loss [64,50,9] had negligible effect, as very little mass had been lost at the time of first dredge-up (or at the time of second dredge-up, in intermediate mass stars).

Models of "extra mixing" and the consequent cool bottom processing on the RGB [81,19,87,22,9,69] generally contain free parameter(s) to control the depth and/or speed of the mixing, whose values may be determined by matching observed RGB stellar compositions. Models presented in this work [87,9,69] use a simple "conveyor-belt" circulation scenario, where the extra mixing reaches down into the outer wing of the H-burning shell. The temperature difference $\Delta \log T$ between the bottom of mixing and the bottom of the H-burning shell was considered a free parameter (with a value

$\Delta \log T \approx 0.26$ obtained by requiring a $Z = 0.02$, $1.2\,M_\odot$ case to reproduce the average observed $^{12}C/^{13}C$ ratio). Changes in the envelope structure were followed as the star climbs the RGB, by using the structure from a stellar evolutionary run without extra mixing (as the effect of the extra mixing on the envelope structure should be small). For carbon and heavier elements, the speed of circulation is irrelevant within wide limits (a larger number of rapid circulation passes has the same effect as a smaller number of slow ones; note that if a diffusive approach to mixing had been used, as by Denissenkov & Weiss [22], then the choice of the speed of mixing would have had a greater effect on the nucleosynthesis).

Charbonnel [19] has attempted to go one step beyond parameterized models such as the one described above, by basing models of extra RGB mixing on Zahn's [91] prescription for transport of chemicals and angular momentum in rotating stars that are losing angular momentum due to a stellar wind. Zahn's [91] approach is similar to that of Pinsonneault [63], assuming a reasonable functional form for the mixing instabilities and parameterizing them in terms of a few adjustable parameters. However, rather than treating all transport as diffusive, Zahn assumes that meridional circulation can transport both chemicals and angular momentum, but that shear instabilities lead to largely horizontal turbulence, homogenizing the star at each radial layer and thus converting the transport of chemicals to a much slower diffusive process with diffusion constant $D \approx C_h \frac{3}{80\pi} |\frac{dJ}{dt}| \frac{1}{\alpha\rho\Omega r^3}$, where $\alpha = \frac{1}{2} \frac{d\ln r^2\Omega}{d\ln r}$, $\Omega$ is the local angular velocity, $\frac{dJ}{dt}$ is the rate of loss of angular momentum due to a stellar wind, and $C_h$ is an adjustable parameter $\lesssim 1$ — on the main sequence, Zahn [91] estimates $C_h \approx 0.15$ from the observed extent of Solar lithium depletion. Charbonnel [19] assumed $C_h = 1$, with a constant and depth-independent angular rotation velocity $\Omega$ corresponding to a reasonable surface rotation velocity of $1\,\mathrm{km\,sec^{-1}}$ on the RGB, and a Reimers' [64] mass loss using $\eta = 0.11$ for $Z = 0.001$ and $\eta = 0.035$ for $Z = 0.0001$ in stars of 0.8 and $1\,M_\odot$. The mixing was assumed to reach down to the "top of the H-burning shell" [19], presumably determined by the stabilizing effect of the molecular weight gradient [82] in the outer wing of the H-burning shell. Whether the above assumptions, and Zahn's parameterization of rotational mixing itself, are appropriate on the RGB can only be determined by comparison with the observations, as he noted himself [91].

A desirable goal, which has not yet been attempted by any author, would be a self-consistent model of angular momentum transport, differential rotation, and the consequent extra mixing throughout a star's interior during its lifetime (main sequence and RGB, at the least), using a theoretical prescription of rotational mixing such as that of Zahn [91] or of Pinsonneault [63]. Complicating such an attempt would be the possibility that the parameter values — or even the parameterization — appropriate to the main sequence might require changes to correctly describe the RGB.
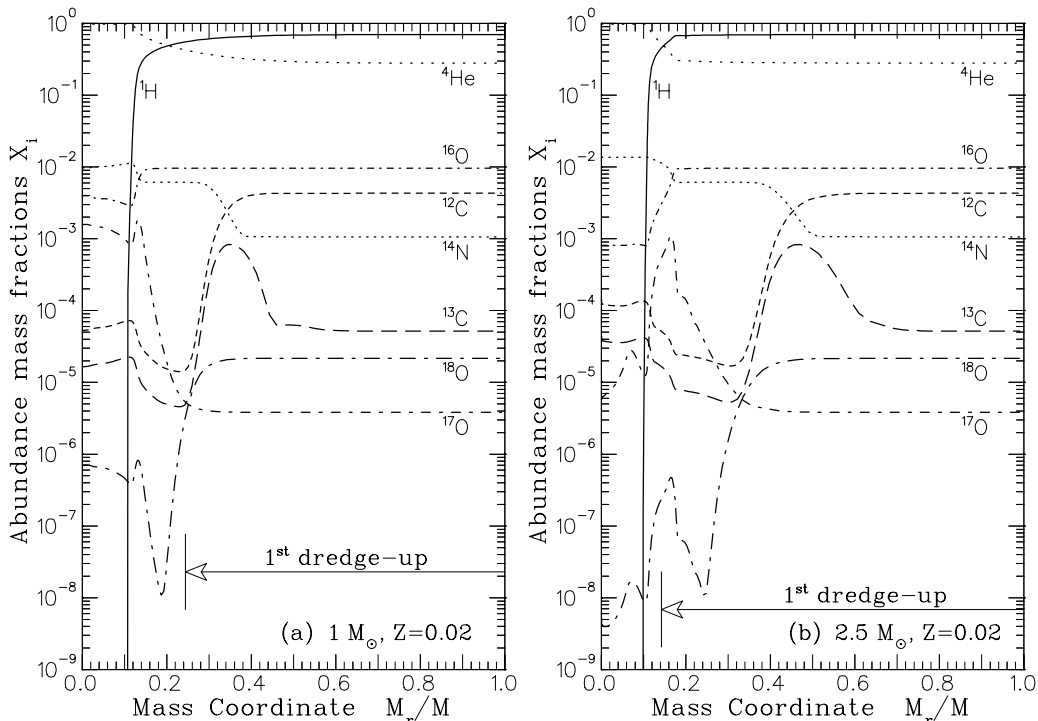
**FIGURE 3.** Composition profiles as a function of the normalized mass coordinate, for stars near the base of the RGB (prior to first dredge-up); the depth later reached by first dredge-up is indicated by the horizontal arrow at the bottom. (*a*) 1.0 $M_\odot$ star, (*b*) 2.5 $M_\odot$ star; both with solar metallicity ($Z = 0.02$).

During core H-burning on the main sequence, partial H-burning in the outer core produces a region of altered abundances (see Fig. 3); as the star approaches the RGB and a deep convective envelope develops, this region is engulfed and mixed into the envelope (*first dredge-up*). Li, Be, and B have been destroyed in all but the outer layers of the star. Partial *p*-*p* chain burning has left a pocket rich in $^3$He. Slightly further in, most of the $^{15}$N has been destroyed, and a $^{13}$C-pocket exists, where $^{12}$C/$^{13}$C approaches its nuclear equilibrium ratio of $\sim 3$, but only part of the $^{12}$C has been burned. Below, most of the $^{12}$C and $^{13}$C have been converted into $^{14}$N, $^{18}$O has been destroyed, and $^{17}$O begins to be enhanced from partial burning of $^{16}$O.

As the $^{13}$C-pocket is engulfed by the convective envelope, the surface $^{12}$C/$^{13}$C ratio is reduced from its large initial value ($\sim 90$ for solar compositions) to $\sim 30$ in low mass stars and somewhat less ($\sim 20$) in intermediate mass stars (see theoretical curves of Fig. 4). However, as shown in Figure 4, observations of RGB and post-RGB $^{12}$C/$^{13}$C ratios in galactic open clusters [31] indicate the an increasing trend with stellar mass, not a decreasing one.

Gilroy & Brown [32] observed $^{12}$C/$^{13}$C ratios as a function of luminosity on the RGB. They found that observed and theoretical ratios agree very well up to and somewhat past the point of deepest first dredge-up, but that excess
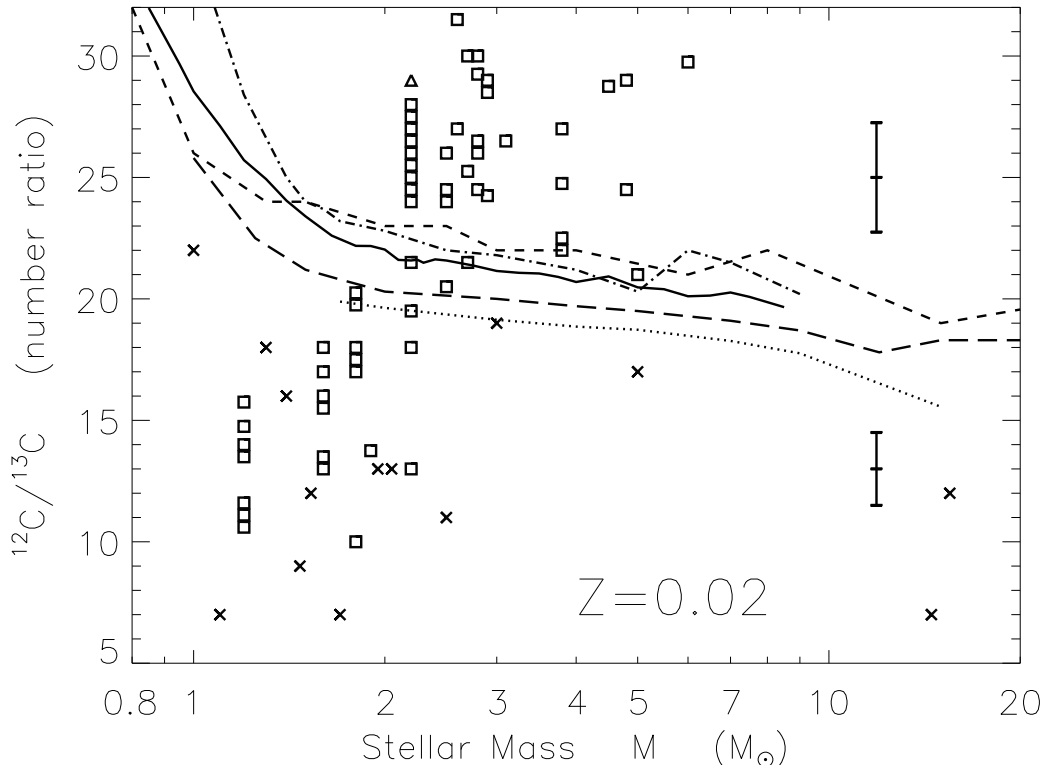
**FIGURE 4.** Comparison of observed stellar $^{12}$C/$^{13}$C ratios with theoretical first dredge-up predictions of various authors (for stars of solar metallicity). *Squares*: galactic open cluster observations [31] (error-bars at right of plot show typical observational error; *triangle* indicates lower limit), having accurate determinations of the stellar mass. *Crosses*: isolated star observations [34,35,38], with masses uncertain by a factor of $\sim 2$. Theoretical curves: *solid*: Boothroyd & Sackmann [9], *dotted*: El Eid [23], *short-dashed*: Dearborn [20], *long-dashed*: Schaller *et al.* [74] and also Charbonnel [18], *dot-dashed*: Bressan *et al.* [13].

$^{13}$C began to appear after the point where the H-burning shell reached the composition discontinuity that was left behind by deepest first dredge-up. As discussed by Charbonnel [18], this is consistent with cool bottom processing due to relatively slow (weak) extra mixing, because the mixing instability can be stabilized by a molecular weight gradient: the large molecular weight gradient at the composition discontinuity acts as a barrier to mixing. Once the H-burning shell has reached (and erased) the composition discontinuity, the extra mixing can transport envelope material down into the outer wing of the H-burning shell, where H-burning produces a molecular weight gradient (how deep into the shell the mixing would reach is determined by the details of the mixing mechanism, but can be estimated by the observed nucleosynthetic results at the stellar surface). For stars of mass $> 2~M_\odot$, the end of the RGB occurs before the composition discontinuity has been erased; thus these intermediate-mass stars do not encounter RGB cool bottom processing.
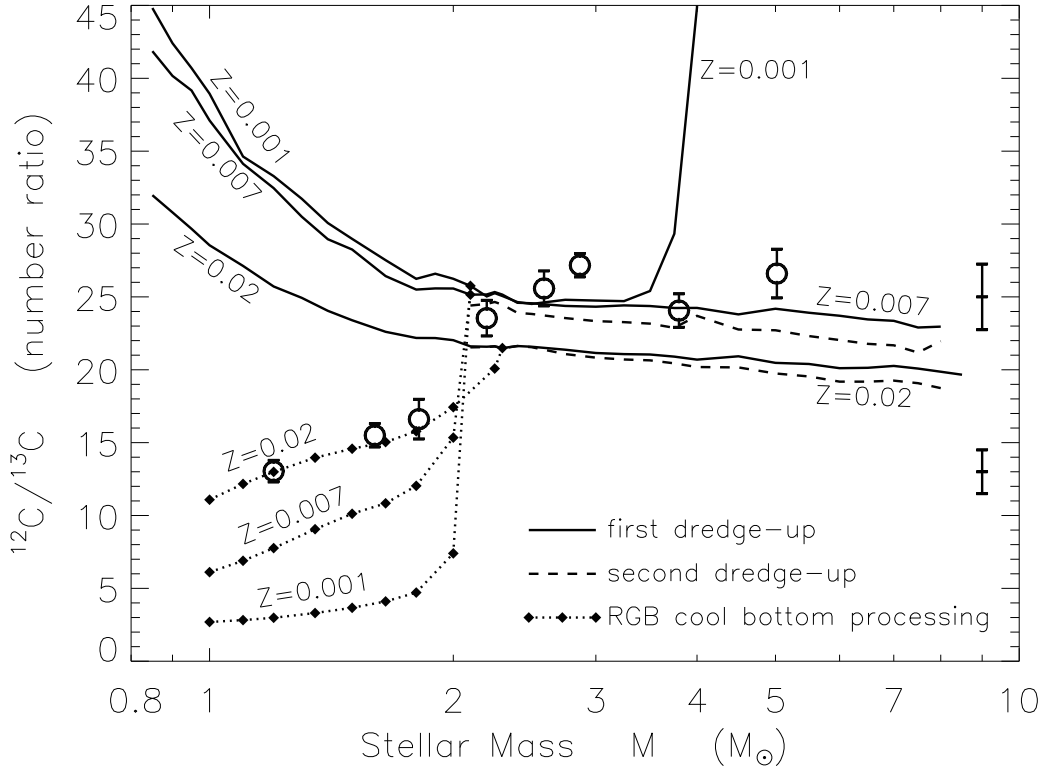
**FIGURE 5.** Theoretical $^{12}C/^{13}C$ ratios resulting from first dredge-up (*solid lines*), cool bottom processing on the RGB (*diamonds*), and second dredge-up on the E-AGB in intermediate-mass stars (*dashed lines*), for three metallicities $Z$ (for clarity, second dredge-up is not plotted for $Z = 0.001$; it coincides approximately with the $Z = 0.007$ case.) Initial stellar $^{12}C/^{13}C$ ratios were assumed to be inversely proportional to Fe/H, as per galactic chemical evolution models of Timmes *et al.* [83,84]. *Open circles* show average ratio from galactic open cluster observations [31], with error-bars showing internal statistical error in the mean (from observational scatter); error-bars at far right show typical observational errors. Note cool bottom processing models were normalized at 1.2 $M_{\odot}$ (for $Z = 0.02$).

In Figure 5, the solid lines show theoretical predictions of the $^{12}C/^{13}C$ ratio resulting from first dredge-up, as a function of stellar mass and metallicity. The trend with stellar mass is due to the fact that low mass stars have narrower $^{13}C$-pockets than intermediate mass stars (the entire $^{13}C$-pocket is always dredged up). The trend of increased $^{12}C/^{13}C$ ratio for reduced metallicity $Z$ is due to the fact that the initial stellar $^{12}C/^{13}C$ ratio was assumed to be inversely proportional to Fe/H [83,84]; models where the initial stellar $^{12}C/^{13}C$ ratio was assumed to be independent of metallicity show a very small trend in the opposite direction (see also Charbonnel [18]). The average observed $^{12}C/^{13}C$ ratios in RGB and post-RGB stars, in galactic open clusters of near-solar metallicity, are shown by the open circles in Figure 5; for stars of mass $> 2 \; M_{\odot}$, they are in reasonable agreement with the theoretical curves,

(although they suggest that the $^{13}$C-pocket may in fact be about 20% smaller than predicted by standard theoretical models). For stars of mass $\lesssim 2\,M_\odot$, the observations reflect the "extra mixing" and cool bottom processing that produces additional $^{13}$C subsequent to first dredge-up. Estimates of the $^{12}$C/$^{13}$C ratio at the tip of the RGB that result from cool bottom processing, with the simple circulation model described above, are shown by the solid diamonds in Figure 5. The depth of the extra mixing in the models is determined by the observed $^{12}$C/$^{13}$C ratio in stars of mass $1.2\,M_\odot$, and thus by definition the cool bottom processing models reproduce that observational point. As expected, given the normalization at $1.2\,M_\odot$, they also reproduce the trend with stellar mass shown by the observations of stars with masses between 1.2 and 2 $M_\odot$. Under the assumption that extra mixing always reaches the same point in the outer wing of the H-burning shell, independent of metallicity, Figure 5 shows that cool bottom processing has a much greater effect on low metallicity (Population II) stars than in stars of near-solar metallicity (Population I). This is due to the fact that CNO-cycle burning proceeds at higher temperatures in the H-shell of a low metallicity star, to compensate for the reduced CNO abundance. If anything, these cool bottom processing models underestimate the effect of metallicity, as discussed below.

The Population II extra mixing models of Charbonnel [19] reproduce the rapid achievement of $^{12}$C/$^{13}$C $\approx$ 3 in the stellar envelope that is observed in such stars. A decline in $^3$He (not observable) and in $^7$Li (consistent with observations) was also reported [19]. This behavior is qualitatively correct, but a quantitative test of the model would require consideration of Population I stars, or of more diagnostic isotopes for such Population II stars, e.g., total carbon or oxygen abundances, or heavier elements such as sodium, magnesium, and aluminum, whose observed behavior on the RGB is discussed below.

Low mass stars ($M \lesssim 2\,M_\odot$), which develop a degenerate helium core, experience a lengthy RGB stage with significant cool bottom processing before the violent ignition of core helium, in the "helium core flash"; stars of higher mass ignite helium quiescently in a non-degenerate core, and experience only a brief RGB stage, with no opportunity for cool bottom processing. In the models of Boothroyd & Sackmann [9], Population II stars of mass $\gtrsim 4\,M_\odot$ ignite core helium before they ever reach the RGB, and thus experience no first dredge-up at all (see the $Z = 0.001$ case of Fig. 5). Whether this "early" core helium ignition actually occurs in higher mass Population II stars is not certain: the corresponding models of Charbonnel [18,24] show only slightly shallower first dredge-up than Population I stars, while the corresponding models of Lattanzio [57] show intermediate behavior. The exact point of core helium ignition in these stars thus appears to be sensitive to details of the physical inputs and/or numerical treatment of the stellar models (as are the form and extent of the "Cepheid loops" experienced by intermediate mass stars during core He-burning). However, any resulting uncertainties in the surface composition are wiped out by second dredge-up on the E-AGB.

As helium begins to burn in a shell surrounding a degenerate carbon–oxygen core, the star begins to climb the AGB and the convective envelope deepens. In low mass stars, the convective envelope does not reach as deep as the H-burning shell, and thus mixes matter that was already homogenized by first dredge-up; the surface composition thus changes very little. In intermediate mass stars, the H-burning shell is extinguished on the E-AGB and second dredge-up reaches down into the H-exhausted material left behind by the H-burning shell. There almost all the CNO isotopes have been converted into $^{14}$N, so dredge-up of this material has little effect on the $^{12}$C/$^{13}$C ratio (see dashed lines in Fig. 5). However, if first dredge-up has not yet mixed the $^{13}$C-pocket to the surface (as may be the case in high mass Population II stars), second dredge-up will do so. Since second dredge-up in intermediate mass stars occurs before any significant amount of mass loss, the composition of the material injected into the interstellar medium is not affected by any uncertainty in first dredge-up for Population II stars.

The envelope $^{14}$N/$^{15}$N ratio is increased from $\sim 250$ to $\sim 1000 - 1500$ by first and/or second dredge-up [23,24], due to the engulfing of $^{15}$N-depleted, $^{14}$N-enriched material. However, any cool bottom processing that significantly affects the $^{12}$C/$^{13}$C ratio should also destroy almost all the $^{15}$N in the star's envelope (yielding the nuclear equilibrium ratio $^{14}$N/$^{15}$N $\gtrsim 10^4$).

Figure 6 illustrates the depletion in total carbon abundance (by a factor of $\lesssim 2$) and the corresponding $^{14}$N enhancement due to first and second dredge-up (the total oxygen abundance is never affected by first or second dredge-up). Figure 6 also shows that, while the RGB cool bottom processing models predict negligible effects on total carbon and nitrogen abundance for near-solar metallicities, large effects are predicted for Population II metallicities (these RGB cool bottom processing models also predict that the total oxygen abundance will not be affected at any metallicity). These models agree with observations of Population II field stars and of some globular clusters (e.g., M4, 47 Tuc, NGC 3201, NGC 2298, NGC 288), which show no oxygen depletion (see, e.g., Kraft [48], and references therein). On the other hand, there are many globular clusters that do show large oxygen depletions on the RGB (e.g., M5, M13, M3, M92, M15, M10, NGC 4833, NGC 362: see [48]), and some globular clusters with metallicities $Z \gtrsim 0.001$ (e.g., 47 Tuc) exhibit RGB carbon depletions of over an order of magnitude, much larger than that in the $Z = 0.001$ model in Figure 6. A change in the normalization of extra mixing, i.e., deeper mixing (down to hotter temperatures), would produce the observed oxygen depletions (as well as the anti-correlation of O with Na and Al also observed in some globular clusters), as shown by the higher-temperature models computed by Denissenkov & Weiss [22]; they found, however, that such models could not simultaneously match the carbon observations (too much carbon was destroyed). This suggests that there is a star-to-star variation in the depth of extra mixing, and possibly a variation in the depth of mixing as the star climbs the RGB. A similar conclusion follows from the
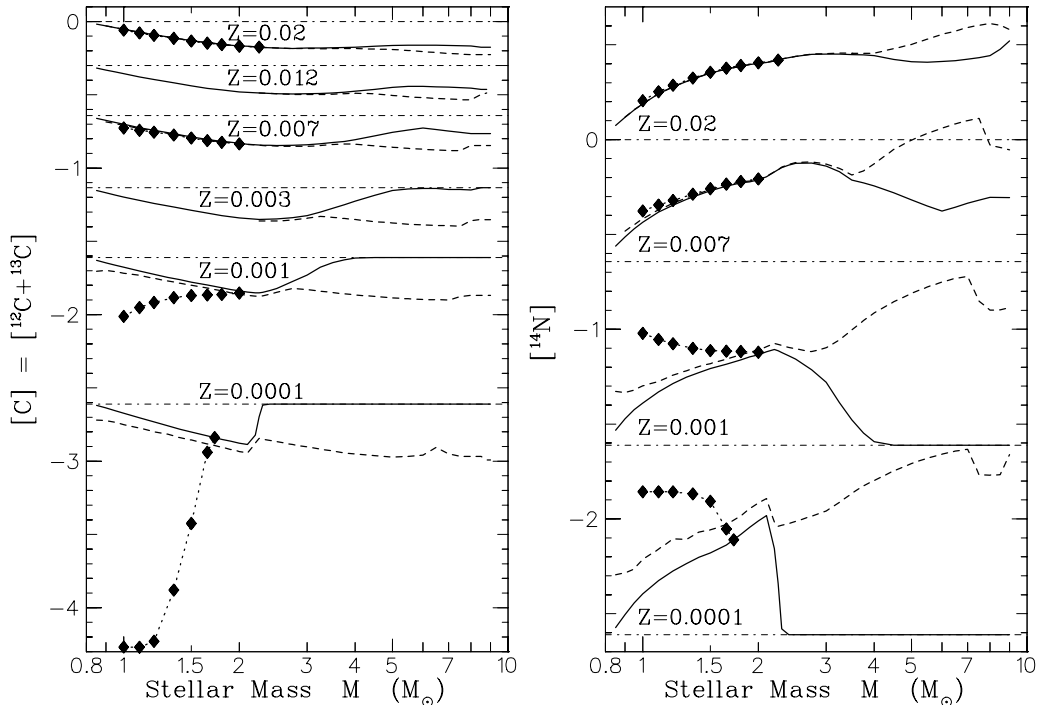
**FIGURE 6.** Predicted carbon depletions and nitrogen enhancements due to first dredge-up (*solid lines*), cool bottom processing on the RGB for $Z = 0.02$, 0.007, 0.001, and 0.0001 (*diamonds*), and second dredge-up on the E-AGB in intermediate-mass stars (*dashed lines*); note that for $Z = 0.02$, 0.007, 0.001, and 0.0001, second dredge-up was also computed for low mass stars, but *without* including any effects of prior RGB cool bottom processing. To avoid confusion, [$^{14}$N] curves for $Z = 0.012$ and 0.003 are omitted. *Dot-dashed lines* indicate initial abundances. Note that $[C] \equiv \log\{n(C)/n(C_\odot)\}$, where number fraction $n(C) \equiv n(^{12}C) + n(^{13}C)$, and that $[^{14}N] \equiv \log\{n(^{14}N)/n(^{14}N_\odot)\}$.

models of Langer *et al.* [53,52]. Note that the oxygen-depletion and Na-Al observations require that, in some stars, extra mixing must reach temperatures corresponding to those at the *bottom* of the H-burning shell in standard stellar models. In a case without extra mixing, O depletion and Na production can take place just outside the burning shell (see, e.g., [16]), but when extra mixing is present higher temperatures are needed to deplete O significantly over the entire envelope on the RGB timescale [22].

Figure 7 shows the effect of first and second dredge-up on the $^{16}O/^{17}O$ ratio. There is no effect for stars of $\sim 1\ M_\odot$, since the convective envelope (during first dredge-up) does not reach the $^{17}O$-pocket in these stars. For $1\ M_\odot \lesssim M \lesssim 2\ M_\odot$, the convective envelope reaches partially into the $^{17}O$-pocket; since there is a steep abundance gradient at the outer edge of this $^{17}O$-pocket, the exact amount of $^{17}O$ dredge-up is sensitive to the precise depth of convection and form of the profile. Thus there is some disagreement between different investigators in this mass range; the predictions for $Z = 0.02$ in Fig-
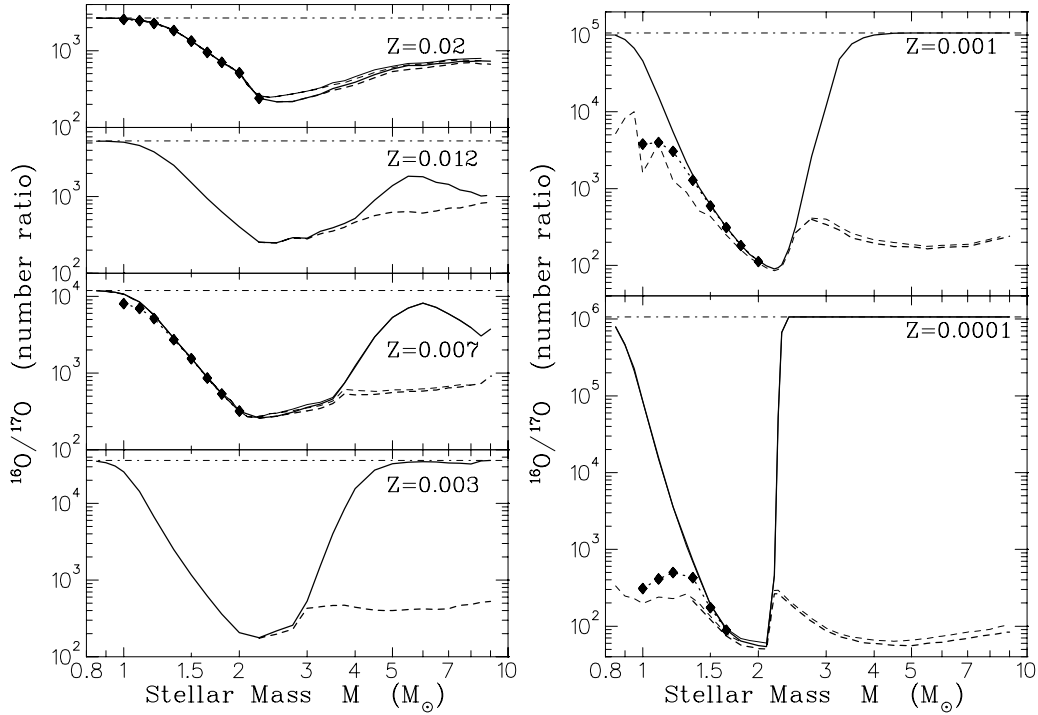
**FIGURE 7.** The $^{16}O/^{17}O$ ratios resulting from first and second dredge-up and RGB cool bottom processing; notation as in Fig. 6. Initial stellar $^{16}O/^{17}O$ ratios were assumed to be inversely proportional to Fe/H, as per galactic chemical evolution models of Timmes *et al.* [84]. The $^{17}O + p$ reaction rates of Landré *et al.* [51] were used in general; the slightly higher $^{16}O/^{17}O$ ratios resulting from the more accurate Blackmon *et al.* [4,3] rates are also shown for $Z = 0.02$, 0.007, 0.001, and 0.0001 (i.e., the upper of the two solid lines, or of the two dashed lines).

ure 7 agree well with those of Bressan *et al.* [13] and Schaller *et al.* [74], but Dearborn [20] finds larger $^{17}O$-enhancements below $1.5\,M_\odot$ (see also discussion by El Eid [23]). For stars of mass $\gtrsim 2\,M_\odot$, the convective envelope reaches down slightly below the peak of the $^{17}O$ pocket, yielding large surface $^{17}O$ enrichments, as shown in Figure 7. In Population II stars, the $^{17}O$ pocket is wider than in Population I stars, leading to more $^{17}O$ enrichment relative to $^{16}O$, although this may not be attained until second dredge-up in higher masses, where first dredge-up may not occur (as discussed above). Uncertainties in the $^{17}O$-destruction rates have no effect below $2\,M_\odot$, because dredge-up does not reach regions where any $^{17}O$ was destroyed; in this mass range, the uncertainties in the stellar observations are too large to say more than that theory and observation are not inconsistent [20,23,11]. For $M \gtrsim 2\,M_\odot$, differences between the $^{16}O/^{17}O$ results of different investigators are largely due to use of different rates for the $^{17}O$-destruction reactions, as discussed by El Eid [23] (see also [11]). The most recent $^{17}O + p$ rates of Blackmon *et al.* [4,3] have much smaller uncertainties; they differ by about 2-$\sigma$ (in the "uncertain fac-
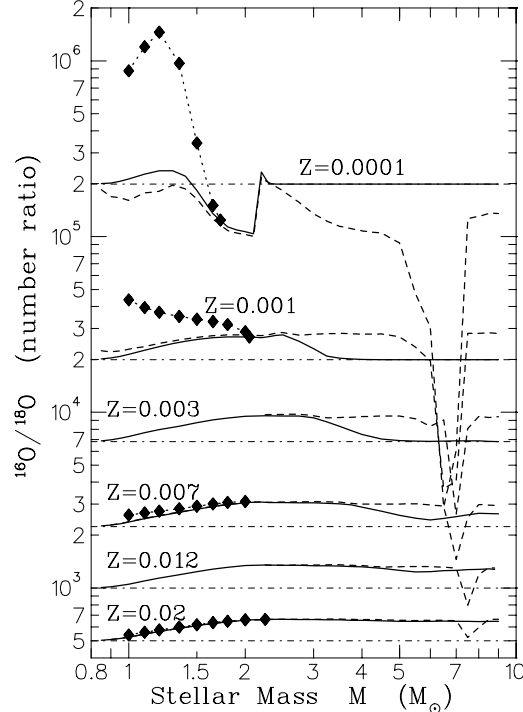
**FIGURE 8.** The $^{16}O/^{18}O$ ratios from first and second dredge-up and RGB cool bottom processing; notation as in Fig. 6. Initial stellar $^{16}O/^{18}O$ ratios were assumed to be inversely proportional to Fe/H, as per Timmes *et al.* [84].

tor $f_1$") from the previous recommended rates of Landré *et al.* [51], and yield abundances that differ by less than 20%, as shown in Figure 7 (both being consistent with observations of intermediate mass stars [11]). Except for stars of very low mass ($\lesssim 1\ M_\odot$), the final $^{16}O/^{17}O$ ratio is almost independent of its initial value, as one would expect, since the amount of $^{17}O$ dredged up is much larger than the amount originally present in the envelope.

Figure 7 shows that cool bottom processing on the RGB should have little effect for Population I stars, but should yield quite large $^{17}O$ enhancements in low mass Population II stars — comparable to the $^{17}O$ enhancements that would result from second dredge-up in the *absence* of cool bottom processing. Some Population II stars experience significant $^{16}O$ depletion on the RGB (this is observed in some globular cluster stars: see above); for such stars, where the models of the present work underestimate the extent of cool bottom processing, the $^{16}O/^{17}O$ ratio should approach CNO-cycle equilibrium, namely, $100 \lesssim {}^{16}O/^{17}O \lesssim 500$ for the relevant H-burning temperatures.

Since the amount of $^{18}O$-depleted matter engulfed by first and/or second dredge-up is never a very large fraction of the total envelope mass, dredge-up usually does not change the surface $^{18}O$ abundance much, as may be seen from Figure 8; this agrees with RGB observations [11]. The only exception to this is in stars of $\sim 7\ M_\odot$, where second dredge-up may reach material
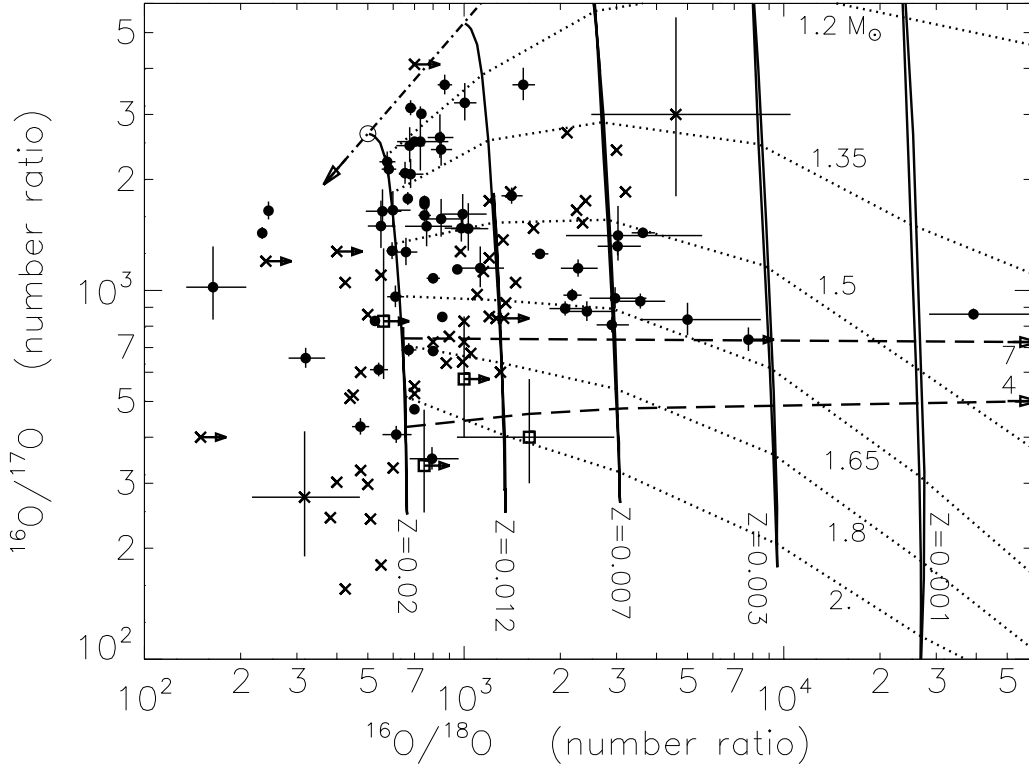
**FIGURE 9.** The oxygen isotope–isotope diagram. *Dot-dashed line*: evolution of the inter-
stellar medium [84] (*open circle*: solar ratios). *Solid lines* (labelled by $Z$) give the theoretical
locus occupied by first and second dredge-up abundances. *Dotted lines* give first dredge-up
abundances for six stellar masses (as labelled). *Dashed lines* show the effect of TP-AGB hot
bottom burning in $Z = 0.02$ stars of 4 and 7 $M_\odot$. *Crosses*: observed ratios in S and C stars
on the AGB [37,36,47] (typical errors shown for two stars, at lower left and upper right).
*Open squares*: observed ratios in four J-type carbon stars, with $^{12}C/^{13}C \sim 3$ suggesting hot
bottom burning. *Solid circles*: high precision grain measurements [42,41,62,61].

containing $^{18}O$ produced during core He-burning. The *fractional* change in
$^{16}O/^{18}O$ owing to first and second dredge-up is generally almost independent
of the initial $^{16}O/^{18}O$ ratio. Figure 8 also demonstrates that $^{18}O$ is essentially
unaffected by cool bottom processing in solar metallicity stars on the RGB,
but can be significantly depleted in Population II RGB stars of low mass.

While low-mass solar-metallicity stars experience little $^{18}O$ depletion on the
RGB, there is some observational evidence that suggests that they may ex-
perience significant $^{18}O$ depletion (or $^{16}O$ enhancement) on the AGB [87,9].
Figure 9 shows oxygen isotope ratios observed in AGB stars known to be in the
TP-AGB phase (from the fact that they are S stars or C stars, and thus must
have experienced third dredge-up). There appears to be a trend, such that
those stars whose $^{17}O$ abundances indicate low masses have higher $^{16}O/^{18}O$
ratios than expected. The indicated $^{18}O$ depletions are not much larger than

the observational errors, but are exhibited by a number of stars. One might suggest that the trend was in fact an age effect, i.e., that low mass stars tend to be older, and thus tend to have lower initial metallicity and lower initial $^{18}$O abundances; however, no such trend with stellar mass is visible in the (admittedly few) RGB oxygen isotope observations. The high precision grain data (solid circles in Fig. 9) certainly show a wide range in $^{18}$O abundances. Only four of the most $^{18}$O-depleted grains have abundances consistent with an origin in a 7 $M_\odot$ star that is undergoing hot bottom burning on the AGB (see section VI and dashed lines in Fig. 9). To explain the rest by variations in the initial isotope ratios would require that these grains originated in $\sim 1.6\ M_\odot$ stars with metallicity $\sim 1/3$ of solar — not impossible, but not what one would have expected, since most of the other grains exhibit $^{16}$O/$^{18}$O ratios indicative of metallicities > 2/3 of solar. It has been suggested that $^{18}$O depletions in low mass AGB stars would occur naturally if the extra mixing/cool bottom processing mechanism operated in at least some AGB stars [12,87] (as well as RGB stars). If this were the explanation for the AGB $^{18}$O depletions, then the extra mixing on the AGB would have to reach significantly deeper into the H-burning shell than was the case on the RGB, in order to yield significant $^{18}$O depletions on the short AGB timescale. Such stars would be expected to have $^{12}$C/$^{13}$C ratios not far above the nuclear equilibrium value of 3, and to convert significant amounts of $^{12}$C into $^{14}$N, yielding nitrogen enrichments and making it harder to become a carbon star; stellar observations show little or no indication of these other consequences of AGB cool bottom processing, though there is insufficient data to rule out AGB cool bottom processing. An alternative explanation is suggested by a parameterized convective overshoot model of Herwig *et al.* [39], which suggested that third dredge-up could yield significant enrichment of envelope $^{16}$O (in contrast to standard mixing models); if this were the case, the $^{16}$O/$^{18}$O ratio might increase (by a factor of $\lesssim 2$) due to third dredge-up (the $^{16}$O/$^{17}$O ratio would increase slightly less, as some $^{17}$O is produced in the H-shell).

## IV   THERMALLY PULSING-AGB EVOLUTION

The details of AGB evolution have been the subject of much theoretical work, and are, in one sense, quite well understood. The reader is referred to [46,28,56] for details. In 1981, Renzini & Voli [65] attempted to combine theory and observations into a consistent set of nucleosynthetic yields for low and intermediate mass AGB stars, using parameterized "synthetic" AGB nucleosynthesis models. Recently, several authors have used more extensive observations and updated stellar evolution models in a similar manner, to provide improved sets of AGB nucleosynthetic yields [59,85,24]. As discussed below, there are still sufficient uncertainties in AGB evolution that such calculated yields should be taken with a grain of salt, particularly for the elements
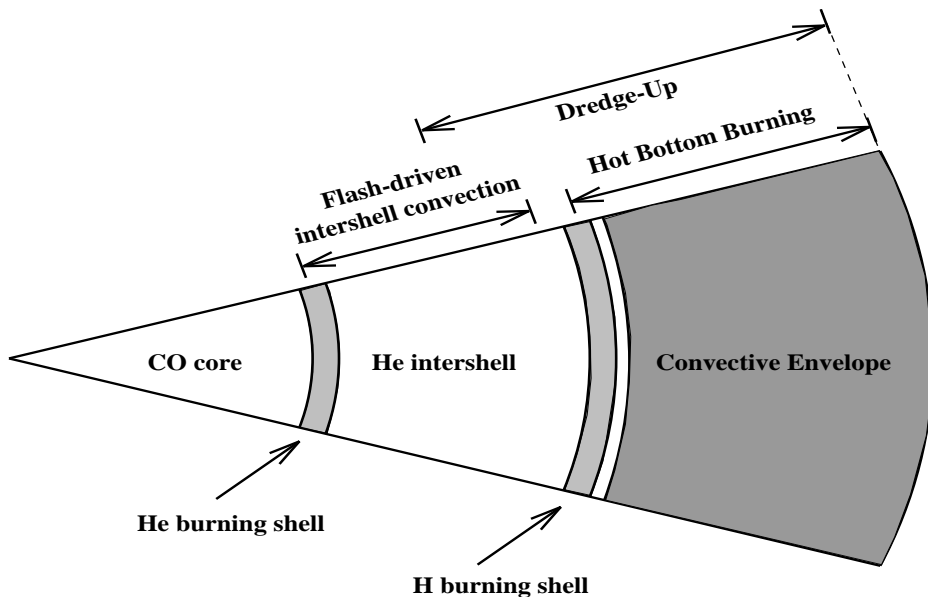
**FIGURE 10.** Schematic structure of an AGB star (**not** to scale). During a thermal pulse the intershell convection extends over the region marked by "flash-driven intershell convection". During the dredge-up phase, the convective envelope moves inward to the depth marked by "dredge-up". For massive stars, during the interpulse phase the convective envelope penetrates the top of the H-shell, so that envelope convection extends down to the region marked "hot bottom burning".

heavier than oxygen, where nuclear rate uncertainties can be considerable [2].

Briefly, an AGB star has the structure shown in Figure 10. The C-O core is the result of He burning, and will become the final white-dwarf remnant. Just above this is the He-shell. This is thermally unstable, and burns vigorously during shell flashes (or thermal pulses) but is essentially extinguished between them. Above the He-shell is the intershell region, so-called because it is between the He and H-shells. Above the H-shell is the convective envelope. During a thermal pulse, the He-shell will deliver some $10^7$ $L_\odot$ for a brief period, and this enormous energy production results in the formation of a convective zone. This "flash-driven intershell convection" extends over the region shown in Figure 10, and thus mixes the products of (partial) He-burning throughout this region. The approximate composition of this zone is 25% $^{12}$C and 75% $^4$He (note, however, that a parameterized convective overshoot model of Herwig *et al.* [39] has yielded a composition 50% $^{12}$C, 25% $^{16}$O, and 25% $^4$He, suggesting that uncertainties in convective mixing can have a significant effect on flash nucleosynthesis: see section V). There are also significant overabundances of $^{22}$Ne, produced via $^{14}$N$(\alpha, \gamma)^{18}$O$(\alpha, \gamma)^{22}$Ne (note that the H-burning shell has converted almost all the CNO elements into $^{14}$N), and of the results of neutron-capture nucleosynthesis, namely, $^{19}$F and "$s$-process isotopes"; $^{19}$F is produced when protons from $(n, p)$ reactions allow the re-

action pathway $^{18}O(p,\alpha)^{15}N(\alpha,\gamma)^{19}F$ to proceed [25,60,24,88]. Following the pulse, the helium luminosity decreases and the star expands. This essentially extinguishes the H-shell, and the bottom of the convective envelope moves inwards in mass. After a small number of pulses, this convection penetrates the region that was mixed by the flash-driven convective zone; this results in the mixing of freshly produced carbon to the stellar surface (*"third dredge-up"*). As the star begins to contract back to its normal configuration, the H-shell is re-ignited and provides all of the energy during the next interpulse phase, until the following pulse.

For more massive stars (above $\sim 4~M_{\odot}$) the bottom of the convective envelope penetrates into the top of the H-shell, and some nuclear reactions take place at the bottom of the convective envelope. This is known as "hot bottom burning" (hereafter HBB), and is shown schematically in Figure 10. The AGB phase terminates when mass loss has reduced the star's envelope mass almost to zero. In the calculations presented below we used the mass loss formula of Vassiliadis & Wood [86], although there are other formulations and the number of thermal pulses, HBB nucleosynthesis, and final stellar mass depend sensitively on this rather uncertain input (see also [10,5,24,79]). The other main sources of uncertainty in AGB evolution are possible errors in low-temperature molecular opacities [67,8,10], and uncertainties in the treatment of convective mixing (see section V).

The repeated operation of the thermal pulse cycle described above is responsible for the periodic addition of carbon to the stellar surface. A crucial parameter in this evolution is the amount of dredge-up, as measured by the so-called "dredge-up parameter" $\lambda = \Delta M_{dredge}/\Delta M_H$, where $\Delta M_{dredge}$ is the amount of matter dredged-up following a given pulse, and $\Delta M_H$ is the amount of matter processed by the H-shell between pulses. These parameters are defined in Figure 11. If enough pulses occur (with sufficient dredge-up per pulse) eventually the star becomes a Carbon star, with $n(C) > n(O)$. These stars are very important for the interpretation of meteoritic grains because it is believed that most SiC grains form in their carbon-rich envelopes. But this production of carbon is really on the tip of the nucleosynthetic ice-berg! We shall deal with some of the other nucleosynthesis products below. For information about the production of fluorine, however, please refer to [60,24].

Neutron capture nucleosynthesis in AGB stars is well known, both observationally and theoretically. We now believe that the neutron source active in these stars (at least the lower masses) is $^{13}C$. But how exactly does this $^{13}C$ arise? This remains a serious problem for the models, which do not exhibit the required $^{13}C$ production. While it is true that some $^{13}C$ is produced by CNO cycling in the H-shell, this is nowhere near enough to produce the neutron exposures inferred from observations of these stars. We will make an *ad hoc* assumption that some kind of extra mixing takes place at the bottom of the convective envelope during the dredge-up phase. This has indeed been found in one of the models of Iben & Renzini [44,45], but has not been reproduced

(a) One thermal pulse.



(b) Two consecutive thermal pulses
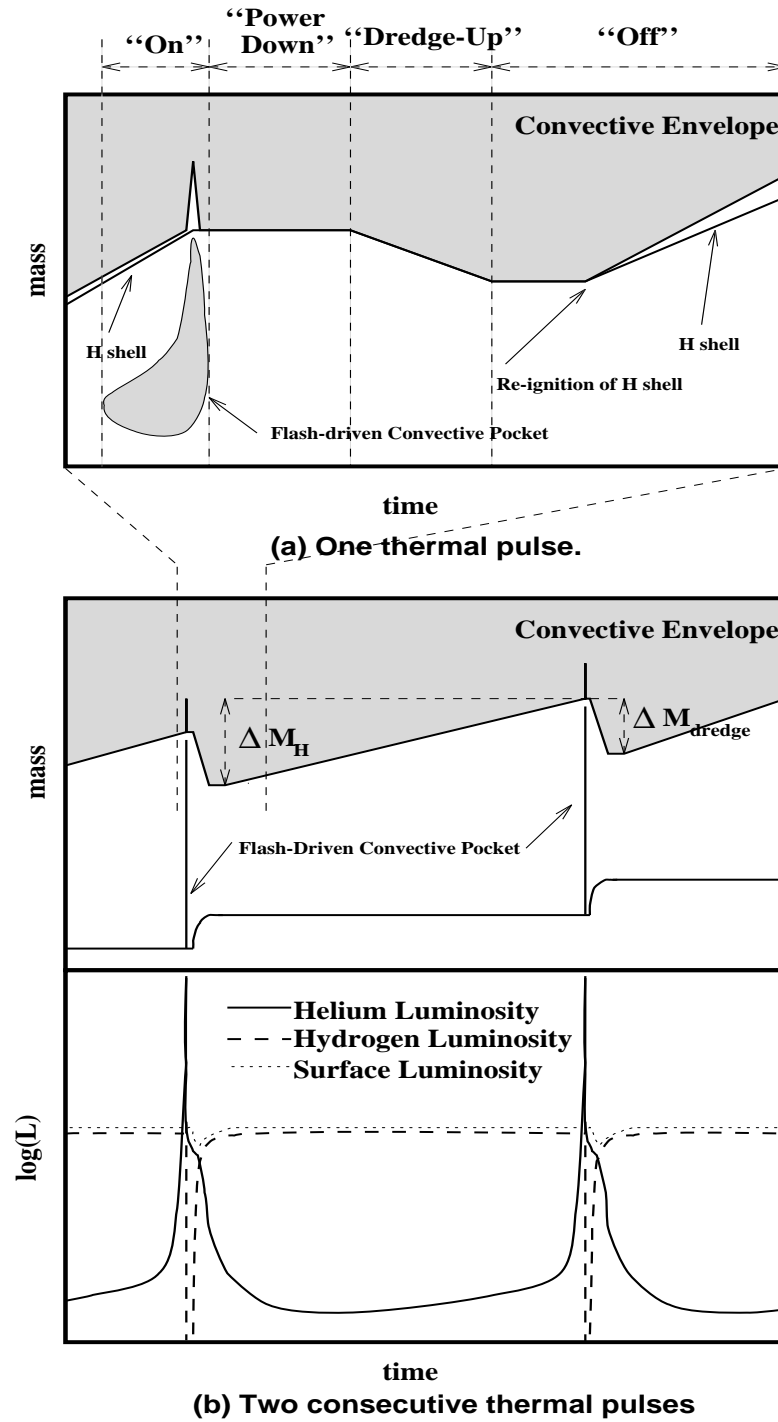
**FIGURE 11.** The four phases of a thermal pulse. In figure (a) we see the detailed evolution during a thermal pulse, showing the intershell convection zone and the dredge-up which follows the pulse. Figure (b) shows two consecutive pulses, and defines the two masses $\Delta M_H$ and $\Delta M_{dredge}$. These define the dredge-up parameter $\lambda = \Delta M_{dredge}/\Delta M_H$. The bottom panel shows the typical luminosity variations during a flash cycle.
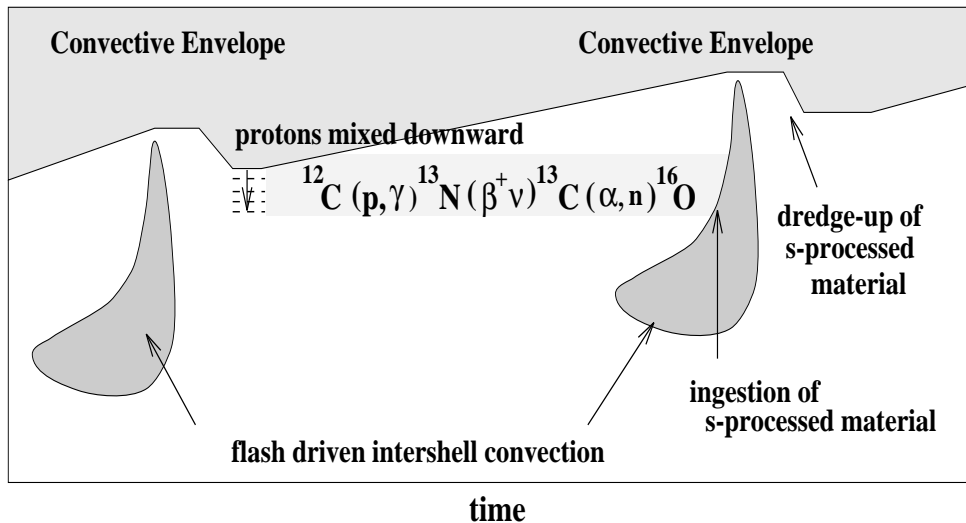
FIGURE 12. Schematic structure of two consecutive thermal pulses, showing how the downward mixing of hydrogen leads to the production of $^{13}$C and then $s$-processing. Note that this $s$-processed material is later dredged to the surface of the star.

by their subsequent models [43], nor by the models of other authors. However, such partial mixing at the base of the envelope convective arises naturally from hydrodynamic simulations of overshoot below a convective region [40,66,27] (and with a parameterization of such an overshoot model, Herwig $et$ $al.$ [39] did indeed find that a $^{13}$C-pocket was produced). Assuming that such mixing does indeed occur, small amounts of hydrogen are mixed into a region which is relatively rich in $^{12}$C. During the subsequent interpulse phase, these regions heat and the protons are captured by the $^{12}$C to produce $^{13}$C. (It is crucial that there is not too much hydrogen in this region, or all the $^{13}$C will be burned to $^{14}$N.) This "$^{13}$C-pocket" was initially believed to sit in the star and wait until the next thermal pulse, when it would be engulfed by the intershell convection. The high temperatures present would then release the neutrons and the $s$-processing would occur in the convective intershell region. But it has been shown recently (Straniero $et$ $al.$ [80], followed by [56,60]) that the temperatures in the intershell are sufficiently high (i.e., the interpulse duration is sufficiently long) that almost all of the $^{13}$C burns to $^{16}$O there, releasing the neutrons locally and thus resulting in $s$-processing $in$ $situ$ with large neutron exposures. Later, when this region is mixed into the flash-driven convection zone, the results of the neutron captures are also mixed into the convective zone. This situation is shown schematically in Figure 12. A brief pulse of neutrons from the $^{22}$Ne neutron source, at the peak of the shell flash, may redistribute $s$-process yields somewhat in the flash-driven convection zone. The details of the $s$-processing are covered in the excellent review by Gallino $et$ $al.$ [30]; $s$-process models (parameterized by the size of the $^{13}$C-pocket) can yield a good match with observed $s$-process abundances.

# V   THE THIRD DREDGE-UP

The nucleosynthesis described above results in changes in the photospheric composition because of the operation of the third dredge-up. Yet there are several details concerning this mechanism which are not well understood. One usually applies the Schwarzschild criterion to determine the convective boundary. This relies on finding the position where the acceleration of gas eddies is zero, which is where $\nabla_{rad} = \nabla_{ad}$. Convective eddies will still have a non-zero momentum when they reach this boundary, and hence they will penetrate into the radiatively stable region where they are decelerated to zero velocity ("*convective overshoot*"). But for third dredge-up, the boundary is even more prone to mixing. The minimum value of $\nabla_{rad}/\nabla_{ad}$ (at the bottom of the convective envelope) exceeds unity substantially, and hence a finite buoyancy will drive eddies into the stable region. Exactly how the star will mix, to achieve the expected convective neutrality, is uncertain. It is, of course, a hydrodynamical problem. We expect the convective region to grow into the intershell region, until the gradients smoothly approach each other. From this configuration we would still expect the usual overshoot.

This situation has been investigated in some detail by [29] who found that the depth of dredge-up depends critically on assumptions made at the boundary of the convective region, as well as on the way in which the mixing is handled within the evolutionary calculation (e.g., if the mixing is performed after each iteration, or only after a model has converged); increasing the number of mass zones and time steps in the model can also have a significant effect [79]. Current work in progress has shown that the depth of dredge-up dramatically alters the evolution of the star. Deep dredge-up cools the intershell region, and slows the advance of the He-shell to almost zero, yielding almost stationary shell burning. The depth of the dredge-up depends also on the treatment of the entropy cost of mixing dense material upward in a gravitational field [90]. Hydrodynamic simulations of stellar convection in 2-D and 3-D have been used in attempts to parameterize the extent of overshoot below a convective envelope that results from the downward plumes typically found in such simulations (e.g., [40,66,27]). Herwig *et al.* [39] applied the overshoot parameterization of [27] to all boundaries of all convective regions, finding significant effects on thermal pulse nucleosynthesis and dredge-up. We have much to learn about this complicated phase of evolution, and work is continuing.

# VI   HOT BOTTOM BURNING

Hot Bottom Burning (hereafter "HBB") is the colourful name given to the circumstance where the temperature at the bottom of a star's convective envelope is sufficiently high for nucleosynthesis to take place. It is perhaps better to think of this as the bottom of the convective envelope penetrating into the

top of the H-burning shell. It is also sometimes known as "convective envelope burning" or simply "envelope burning". The first calculations of HBB were performed by Sackmann *et al.* [72] and Scalo *et al.* [73]; for a discussion of the development and history of this phenomenon, please see [57].

It is only relatively recently that stellar models have shown deep convective envelopes with temperatures exceeding 80 million degrees [6,55] in a thin region at their base. Indeed, it was noticed by [6] that this resulted in the star no longer obeying the core-mass *vs.* luminosity relation, but space prevents us from going into details here (see [6,8,57] for more information).

The first effect of HBB is the production of $^7$Li via the Cameron-Fowler Beryllium Transport Mechanism. The first systematic studies of this were carried out by [68]. The key ingredient is an algorithm for time-dependent mixing because it is essential that the timescale for mixing be much shorter than the electron-capture lifetime for $^7$Be (instantaneous mixing would decrease $^7$Li!). Sackmann & Boothroyd [68] showed that $^7$Li was produced when the temperature $T_{bce}$ at the bottom of the convective envelope exceeded $50 \times 10^6$K, with abundances up to $\log \varepsilon(^7\mathrm{Li}) \sim 4.5$ in stars with $M_{bol} \simeq -6$ to $-7$ (note that $\log \varepsilon(^7\mathrm{Li}) \equiv \log\{n(^7\mathrm{Li})/n(\mathrm{H})\} + 12$); similar results (with slightly higher peak lithium abundances) were obtained in HBB models of Forestini & Charbonnel [24]. This is in excellent agreement with the observations [76,77,1,78] which show Magellanic Cloud AGB stars of $M_{bol}$ between $-6$ and $-7$ to have $\log \varepsilon(^7\mathrm{Li})$ in the range 2.2 to 3.8, and galactic AGB stars with $\log \varepsilon(^7\mathrm{Li}) \lesssim 5$.

One of the main effects of HBB is to take the $^{12}$C which is dredged to the surface and process it into $^{14}$N via the CN cycle. Some $^{13}$C will also be produced, but the overall carbon destruction prevents the star from becoming a carbon star. Detailed calculations of the effect of HBB on CNO elements were carried out by Boothroyd *et al.* [10] (see also [59,24,57]). Significant destruction of $^{12}$C together with production of $^{13}$C and $^{14}$N requires temperatures of at least $80 \times 10^6$K. This was found for masses greater than $\sim 3.5$ to $4\,M_\odot$, depending on the metallicity (increasing as $Z$ increases). These authors expect a maximum luminosity of $M_{bol} \approx -6.4$ for carbon stars, as higher luminosities will result in HBB processing the $^{12}$C into $^{14}$N. Despite the narrowness of the burning layer, the mixing timescale is such that the entire envelope is processed through the burning region many times during the interpulse phase, and the nuclear equilibrium ratio $^{12}$C/$^{13}$C $\approx 3$ (by number) is reached for stars with $M_{bol} \gtrsim -6.3$. Thus there is a narrow region (in luminosity) where stars may be rich in $^{13}$C, prior to further processing of $^{12}$C (and $^{13}$C) into $^{14}$N.

The situation with oxygen isotopes is a little more complicated. The third dredge-up appears to have a negligible effect on the oxygen isotopes, but HBB initially destroys any $^{18}$O which is present, and then follows this by producing some $^{17}$O [12]. The complication comes from the fact that many AGB stars do not seem to fit this pattern. This is despite the fact that extremely precise meteoritic grain analysis [62] reveals isotopic ratios which do fit the results of standard first and second dredge-up models quite well (see [11]). It now

appears that to match the observations of S and C stars we may need to invoke some form of "deep extra mixing" during the AGB evolution (possibly in addition to the first ascent of the giant branch, as discussed in section III).

We mentioned above $^{19}$F enrichment from third dredge-up. If a star is massive enough for HBB to develop, then any $^{19}$F added to its envelope is destroyed by $^{19}$F$(p, \alpha)^{16}$O. Thus stars with enhanced $^{19}$F are presumably lower-mass stars, where HBB does not take place. This is consistent with the fact that they are often carbon stars too. But more can be learned from $^{19}$F. To produce the largest observed enhancements of $^{19}$F seems to require a substantial source of $^{13}$C [60,24], just as is needed for the s-process abundances.

Of particular interest to us at this meeting is the production of $^{26}$Al in AGB stars. During hot H-burning there is some production of $^{26}$Al from the Mg-Al reaction chains. This was studied by [26,88,24] who looked into the dredge-up of any $^{26}$Al produced by the H-shell. They found that enhancements of $^{26}$Al could occur, with $^{26}$Al/$^{27}$Al $\sim 0.001 - 0.01$, reproducing the mean observed isotopic ratios. But to obtain the large enhancements required by some grains would require dredge-up to occur when the stellar envelope mass was very small (thus minimizing the dilution of the dredged-up material). Yet the dredge-up stops when the envelope mass decreases too much (the critical envelope mass for dredge-up is very uncertain). An alternative scenario is that HBB will produce $^{26}$Al in the stellar envelope during the interpulse period.

We close now with some preliminary calculations of HBB from [57]. The calculations are for 6 $M_\odot$ models with three compositions, appropriate to the Sun ($Z = 0.02$), the Large Magellanic Cloud ($Z = 0.008$) and the Small Magellanic Cloud ($Z = 0.004$). Figure 13 shows the results for $Z = 0.02$ (in these figures, "al-6" represents the ground state of $^{26}$Al). The Mg-Al chain is producing $^{26}$Al and $^{25}$Mg is being produced by $^{22}$Ne$(\alpha,$n$)$ reactions in the intershell convective zone, which is dredged to the surface after each pulse. Hence the ratios $^{26}$Al/$^{27}$Al and $^{25}$Mg/$^{26}$Mg both increase. We already see that the high $^{26}$Al/$^{27}$Al ratio of up to 0.05 is in good agreement with the most $^{26}$Al-rich meteorite grains (see the chapters by Hoppe & Ott and Nittler in this volume). Unfortunately, order-of-magnitude uncertainties in some magnesium and aluminum burning reactions yield correspondingly large uncertainties in the resulting abundances of $^{26}$Mg, $^{27}$Al, and particularly in $^{26}$Al [2].

As the envelope mass decreases from mass loss the HBB is shut down but third dredge-up continues. The details of the surface composition in the latter stages of a star's life depend critically on the competition between these effects (e.g., [33]). We find that dredge-up is still strong at the 43rd pulse (when the mass has been reduced to 2.4 $M_\odot$) when we stopped calculations. Figure 13 shows that the C/O ratio is kept below unity (by HBB) but begins to increase again from dredge-up of $^{12}$C once the HBB ceases. Likewise, the $^{12}$C/$^{13}$C and $^{14}$N/$^{15}$N ratios begin to deviate from equilibrium once HBB ends. Although HBB has prevented the model from being a carbon star for most of its lifetime on the AGB, the continuing third dredge-up may yet produce a carbon star,
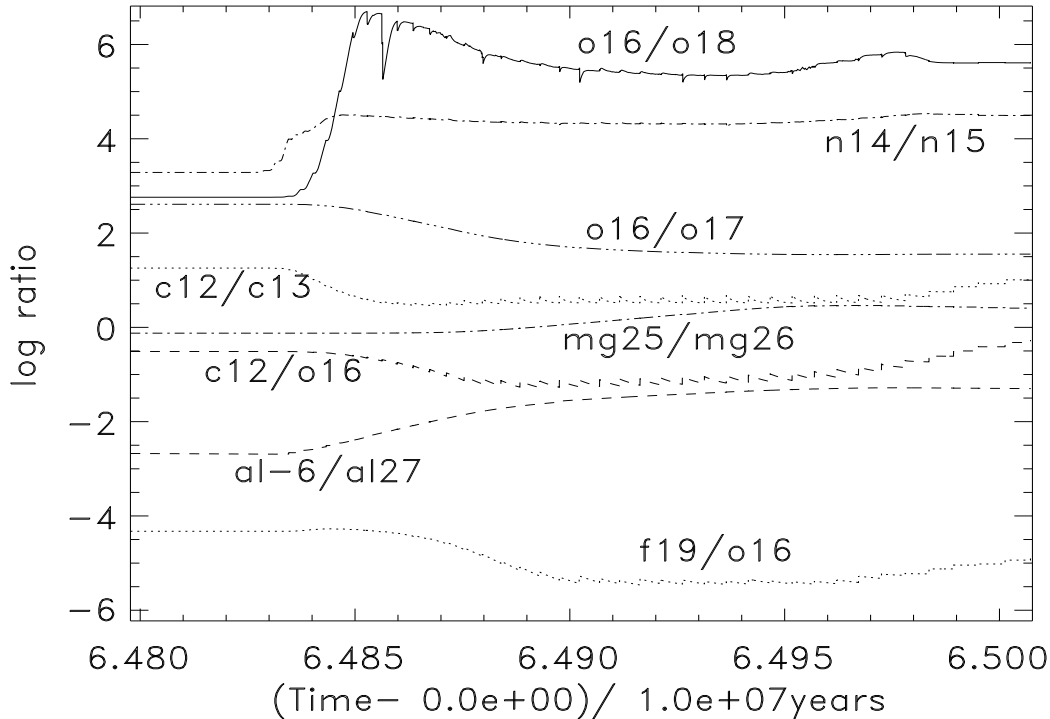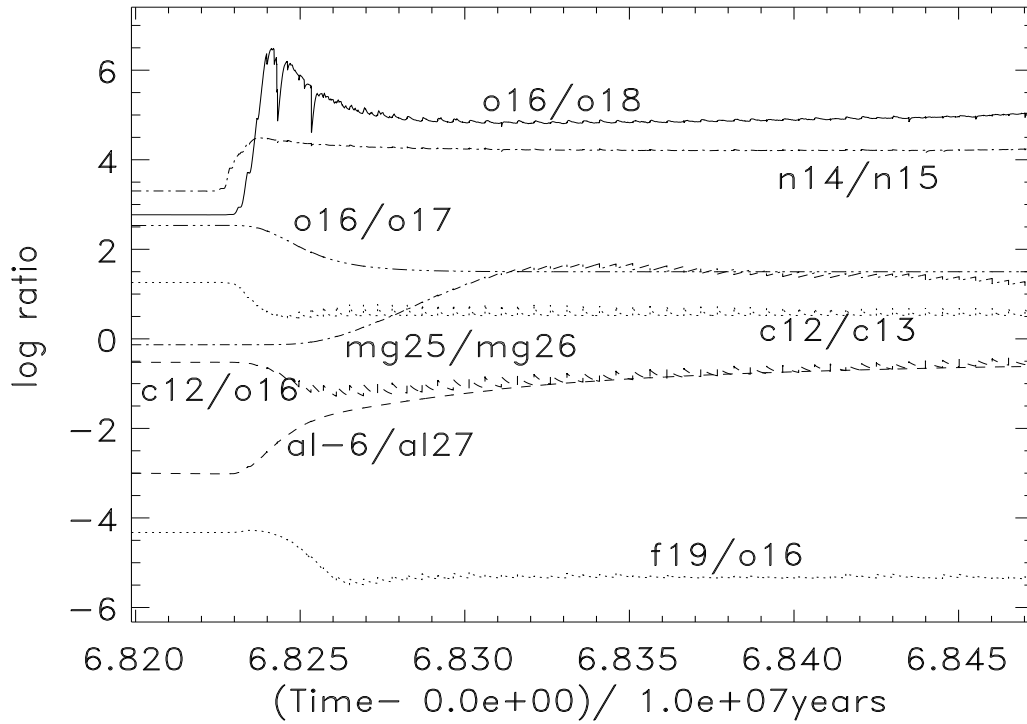
**FIGURE 13.** Surface ratios during the AGB evolution of a 6 $M_\odot$ model with $Z = 0.02$.

but now rich in $^{13}$C. We shall address this point in a later paper.

Figure 14 shows the surface composition for the $Z = 0.008$ model. Dredge-up and HBB are still operating at the end of the calculations shown. Note that $^{26}$Al/$^{27}$Al and $^{25}$Mg/$^{26}$Mg are substantially higher than found for $Z = 0.02$. The ratio $^{12}$C/$^{13}$C is still in equilibrium, although the deep dredge-up is continuing to increase the C/O ratio despite HBB. This star may also become a $^{13}$C-rich carbon star. The surface compositions of the $Z = 0.004$ model are shown in Figure 15. The trends seen in Figure 14 continue here. The model has essentially reached C/O = 1, despite the fact that HBB is still operating, and producing a large amount of $^{13}$C. Note also that we find $^{26}$Al/$^{27}$Al $\simeq 0.6$.

# VII   CONCLUSIONS

In the last decade we have made enormous progress in our understanding of nucleosynthesis and mixing in RGB and AGB stars, and are beginning to understand the origin of pre-solar grains. The rich variety of observations and measurements seem to fit the qualitative pictures described in this paper. Quantitative results are in agreement for some cases, but not all. Our understanding of the processes in the stellar interior that control nucleosynthesis and dredge-up still has several crucial gaps, which will require a great deal of work by experimentalists, observers, and theoreticians to fill in.

**FIGURE 14.** Surface ratios during the AGB evolution of a 6 $M_\odot$ model with $Z = 0.008$.
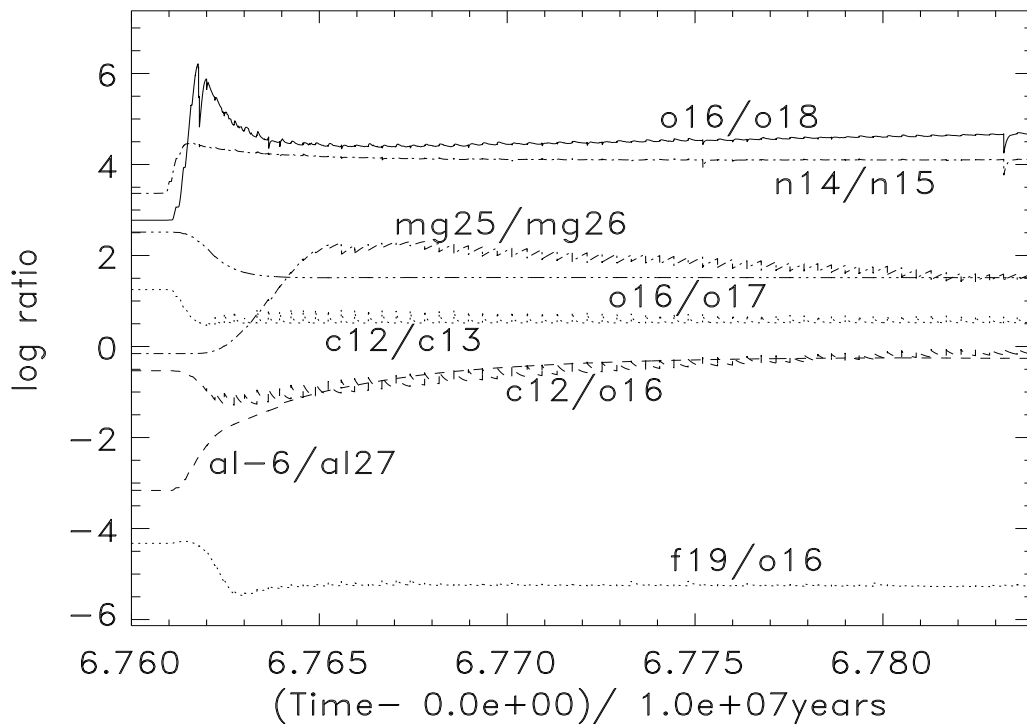


**FIGURE 15.** Surface ratios during the AGB evolution of a 6 $M_\odot$ model with $Z = 0.004$.

# REFERENCES

1. Abia, C., Boffin, H. M. J., Isern, J., & Rebolo, R., *Astron. Astrophys. (Lett.)*, **245**, L1 (1991).
2. Arnould, M., Mowlavi, N., & Champagne, A., in *Stellar Evolution: What Should Be Done?*, Proc. of 32nd Liège Colloquium, ed. A. Noels, D. Frepont-Caro, M. Gabriel, N. Grevesse, & P. Demarque (U. de Liège: Belgium), p. 17 (1996).
3. Blackmon, J. C., private communication (1996).
4. Blackmon, J. C., Champagne, A. E., Hofstee, M. A., Smith, M. S., Downing, R. G., & Lamaze, G. P., *Phys. Rev. Lett.*, **74**, 2642 (1995).
5. Blöcker, T., *Astron. Astrophys.*, **297**, 727 (1995).
6. Blöcker, T., & Schönberner, D., *Astron. Astrophys. (Lett.)*, **244**, L43 (1991).
7. Boothroyd, A. I., & Sackmann, I.-J., *Astrophys. J.*, **328**, 653 (1988).
8. Boothroyd, A. I., & Sackmann, I.-J., *Astrophys. J. (Lett.)*, **393**, L21 (1992).
9. Boothroyd, A. I., & Sackmann, I.-J., *Astrophys. J.*, submitted (1997); preprint astro-ph/9512121.
10. Boothroyd, A. I., Sackmann, I.-J., & Ahern, S. C., *Astrophys. J.*, **416**, 762 (1993).
11. Boothroyd, A. I., Sackmann, I.-J., & Wasserburg, G. J., *Astrophys. J. (Lett.)*, **430**, L77 (1994).
12. Boothroyd, A. I., Sackmann, I.-J., & Wasserburg, G. J., *Astrophys. J. (Lett.)*, **442**, L21 (1995).
13. Bressan, A., Fagotto, F., Bertelli, G., & Chiosi, C., *Astron. Astrophys. Suppl.*, **100**, 647 (1993).
14. Castellani, V., *et al.*, *Astrophys. Space Sci.*, **10**, 340 (1971).
15. Castellani, V., *et al.*, *Astrophys. Space Sci.*, **10**, 355 (1971).
16. Cavallo, R. M., Sweigart, A. V., & Bell, R. A., *Astrophys. J. (Lett.)*, **464**, L79 (1996).
17. Caughlan, G. R., & Fowler, W. A., *Atomic Data Nucl. Data Tables*, **40**, 205 (1988).
18. Charbonnel, C., *Astron. Astrophys.*, **282**, 811 (1994).
19. Charbonnel, C., *Astrophys. J. (Lett.)*, **453**, L41 (1995).
20. Dearborn, D. S. P., *Phys. Reports*, **210**, 367 (1992).
21. Deupree, R. G., 1984, *Astrophys. J.*, **287**, 268 (1984).
22. Denissenkov, P. A., & Weiss, A., *Astron. Astrophys.*, **308**, 773 (1995).
23. El Eid, M. F., *Astron. Astrophys.*, **285**, 915 (1994).
24. Forestini, M., & Charbonnel, C., *Astron. Astrophys. Suppl.*, in press (1997).
25. Forestini, M., Goriely, S., Jorissen, A., & Arnould, M., *Astron. Astrophys.*, **261**, 157 (1992).
26. Forestini, M., Paulus, G., & Arnould, M., *Astron. Astrophys.*, **252**, 597 (1991).
27. Freytag, B., Ludwig, H.-G., & Steffen, M., *Astron. Astrophys.*, **313**, 497 (1996).
28. Frost, C. A., & Lattanzio, J. C., in *Stellar Evolution: What Should Be Done?*, Proc. of 32nd Liège Colloquium, ed. A. Noels, D. Frepont-Caro, M. Gabriel, N. Grevesse, & P. Demarque (U. de Liège: Belgium), p. 307 (1996).

29. Frost, C. A., & Lattanzio, J. C., *Astrophys. J.*, **473**, 383 (1996).
30. Gallino, R., Busso, M., & Lugaro, M., this volume.
31. Gilroy, K. K., *Astrophys. J.*, **347**, 835 (1989).
32. Gilroy, K. K., & Brown, J. A., *Astrophys. J.*, **371**, 578 (1991).
33. Groenewegen, M. A. T., & de Jong, T., *Astron. Astrophys.*, **267** 410 (1993).
34. Harris, M. J., & Lambert, D. L., *Astrophys. J.*, **281**, 739 (1984).
35. Harris, M. J., & Lambert, D. L., *Astrophys. J.*, **285**, 674 (1984).
36. Harris, M. J., Lambert, D. L., Hinkle, K. H., Gustafsson, B., & Eriksson, K., *Astrophys. J.*, **316**, 294 (1987).
37. Harris, M. J., Lambert, D. L., & Smith, V. V., *Astrophys. J.*, **299**, 375 (1985).
38. Harris, M. J., Lambert, D. L., & Smith, V. V., *Astrophys. J.*, **325**, 768 (1988).
39. Herwig, E., Blöcker, T., Schönberner, D., & El Eid, M., *Astron. Astrophys. (Lett.)*, in press (1997).
40. Hurlburt, N. E., Toomre, J., Massaguer, J. M., & Zahn, J.-P., *Astrophys. J.*, **421**, 245, (1994).
41. Huss, G. R., Fahey, A. J., Gallino, R., & Wasserburg, G. J., *Astrophys. J. (Lett.)*, **430**, L81 (1994).
42. Huss, G. R., Hutcheon, I. D., Wasserburg, G. J., & Stone, J., *Lunar Planet. Sci.*, **23**, 563 (1992).
43. Iben, I. Jr., *Astrophys. J. (Lett.)*, **275**, L65 (1983).
44. Iben, I. Jr., & Renzini, A., *Astrophys. J. (Lett.)*, **259**, L79 (1982).
45. Iben, I. Jr., & Renzini, A., *Astrophys. J. (Lett.)*, **263**, L231 (1982).
46. Iben, I. Jr., & Renzini, A., *Ann. Rev. Astron. Astrophys.*, **21**, 271 (1983).
47. Kahane, C, Cernicharo, J., Gómez-González, J., & Guélin, M., *Astron. Astrophys.*, **256**, 235 (1992).
48. Kraft, R. P., *Proc. Astron. Soc. Pacific*, **106**, 553 (1994).
49. Kraft, R. P., Sneden, C., Langer, G. E., & Shetrone, M. D., *Astron. J.*, **104**, 645 (1993).
50. Kudritzki, R. P., & Reimers, D., *Astron. Astrophys.*, **70**, 227 (1978).
51. Landré, V., Prantzos, N., Aguer, P., Bogaert, G., Lefebvre, A., & Thibaud, J. P., *Astron. Astrophys.*, **240**, 85 (1990)
52. Langer, G. E., & Hoffman, R. D., *Proc. Astron. Soc. Pacific*, **107**, 1177 (1995).
53. Langer, G. E., Hoffman, R., & Sneden, C., *Proc. Astron. Soc. Pacific*, **105**, 301 (1993).
54. Langer, G. E., Kraft, R. P., Carbon, D. F., & Friel, E., *Proc. Astron. Soc. Pacific*, **98**, 473 (1986).
55. Lattanzio, J. C., *Proc. Astron. Soc. Aust.*, **10**, 120L (1992).
56. Lattanzio, J. C., Frost, C. A., Cannon, R. C., & Wood, P. R., *Mem. Soc. Astron. Italia.*, **67**, 729 (1996).
57. Lattanzio, J. C., Frost, C. A., Cannon, R. C., & Wood, P. R., in preparation (1997).
58. Lauterborn, D., *et al.*, *Astron. Astrophys.*, **10**, 97 (1971).
59. Marigo, P., Bressan, A., & Chiosi, C., *Astron. Astrophys.*, **313**, 545 (1996).
60. Mowlavi, N., Jorissen, A., & Arnould, M., *Astron. Astrophys.*, **311**, 803 (1996).
61. Nittler, L. R., preprint (1997).

62. Nittler, L. R., Alexander, C. M. O'D., Gao, X., Walker, R. M., & Zinner, E. K., *Nature*, **370**, 443 (1994).
63. Pinsonneault, M. H., Kawaler, S. D., Sofia, S., & Demarque, P., *Astrophys. J.*, **338**, 424 (1989).
64. Reimers, D., in *Problems in Stellar Atmospheres and Envelopes*, ed. B. Bascheck, W. H. Kegel, & G. Traving (New York: Springer), 229 (1975).
65. Renzini, A., & Voli, M., *Astron. Astrophys.*, **94**, 175 (1981).
66. Rieutord, M., & Zahn, J.-P., *Astron. Astrophys.*, **296**, 127 (1995).
67. Sackmann, I.-J., & Boothroyd, A. I., *Astrophys. J.*, **366**, 529 (1991).
68. Sackmann, I.-J., & Boothroyd, A. I., *Astrophys. J. (Lett.)*, **392**, L71 (1992).
69. Sackmann, I.-J., & Boothroyd, A. I., *Astrophys. J.*, submitted (1997); preprint astro-ph/9512122.
70. Sackmann, I.-J., Boothroyd, A. I., & Fowler, W. A., *Astrophys. J.*, **360**, 727 (1990).
71. Sackmann, I.-J., Boothroyd, A. I., & Kraemer, K. E., *Astrophys. J.*, **418**, 457 (1993).
72. Sackmann, I.-J., Smith, R. L., & Despain, K. H. *Astrophys. J.*, **187**, 555 (1974).
73. Scalo, J. M., Despain, K. H., & Ulrich, R. K., *Astrophys. J.*, **196** 805 (1975).
74. Schaller, G., Schaerer, D., Meynet, G., & Maeder, A., *Astron. Astrophys. Suppl.*, **96**, 269 (1992).
75. Smith, G. H., & Tout, C. A., *Mon. Not. Royal Astron. Soc.*, **256** 449 (1992).
76. Smith, V. V., & Lambert, D. L., *Astrophys. J.*, **345**, 375 (1989).
77. Smith, V. V., & Lambert, D. L., *Astrophys. J. (Lett.)*, **361**, L69 (1990).
78. Smith, V. V., Lambert, D. L., Plez, B., & Lubowich, D. A., *Astrophys. J.*, **441**, 735 (1995).
79. Straniero, O., Chieffi, A., Limongi, M., Busso., M., Gallino, R., & Arlandini, C., *Astrophys. J.*, **478**, 332 (1997).
80. Straniero, O., Gallino, R., Busso., M., Chieffi, A., Limongi, M., & Salaris, M., *Astrophys. J. (Lett.)*, **440**, L85 (1995).
81. Sweigart, A. V., & Mengel, J. G., *Astrophys. J.*, **229**, 624 (1979).
82. Talon, S., & Zahn, J.-P., *Astron. Astrophys.*, **317**, 749 (1997).
83. Timmes, F. X., private communication (1995).
84. Timmes, F. X., Woosley, S. E., & Weaver, T. A., *Astrophys. J. Suppl.*, **98**, 617 (1995).
85. van den Hoek, L. B., & Groenewegen, M. A. T., *Astron. Astrophys. Suppl.*, in press; preprint astro-ph/9610030 (1997).
86. Vassiliadis, E. & Wood, P. R., *Astrophys. J.*, **413**, 641 (1993).
87. Wasserburg, G. J., Boothroyd, A. I., & Sackmann, I.-J., *Astrophys. J. (Lett.)*, **447**, L37 (1995).
88. Wasserburg, G. J., Busso, M., Gallino, R., & Raiteri, C. M., *Astrophys. J.*, **424**, 412 (1994).
89. Weaver, T. A, & Woosley, S. E., *Phys. Rept.*, **227**, 65 (1993).
90. Wood, P. R., *Astrophys. J.*, **248**, 311 (1981).
91. Zahn, J.-P., *Astron. Astrophys.*, **265**, 115 (1992).